# Complex Modal Analysis of the Swimming Motion of a Whiting

**B. F. Feeny**[1]
Dynamics and Vibrations Research Laboratory,
Department of Mechanical Engineering,
Michigan State University,
East Lansing, MI 48824
e-mail: feeny@egr.msu.edu

**A. K. Feeny**
Department of Biomedical Engineering,
Johns Hopkins University,
Baltimore, MD 21218
e-mail: afeeny1@jhu.edu

*The kinematics of the transverse motion of a swimming fish are analyzed using a complex modal decomposition. Cinematographic images of a swimming whiting (Gadus merlangus) were obtained from the work of Sir James Gray (1933, "Studies in Animal Locomotion III. The Propulsive Mechanism of the Whiting (Gadus merlangus)," J. Exp. Biol., **10**, pp. 391–402). The position of the midline for each image was determined and used to produce planar positions of virtual markers distributed along the midline of the fish. Transverse deflections of each virtual marker were then used for the complex orthogonal decomposition of modes. This method was applied to images of a whiting before and after amputation in a Newtonian frame of reference and an "anterior-body-fixed" frame as well. The fish motions were well represented by a single complex mode, which was then used as a modal filter. The extracted mode and modal coordinate were used to estimate the frequency, wavelength, and wave speed. The amputated fish was compared to the nonamputated fish, and the amount of traveling in the respective waveforms was quantified. The dominant complex mode shape and the estimated modal frequency were employed to reanimate the fish motion.* [DOI: 10.1115/1.4023056]

## 1 Introduction

We study the kinematics of the swimming motion of a whiting (*Gadus merlangus* or *Merlangius merlangus*) that was examined by Sir James Gray [1,2]. The motion of a fish during swimming is of interest for several reasons. Some species of fish have a natural ability to swim very efficiently. A greater understanding of their movement allows for better appreciation of fish themselves, as well as valuable insight to a very efficient form of underwater locomotion. The work in this area can also be applied to the development of modern technology, such as in biomimetic robotic fish [3–7].

In this paper, we perform complex modal analysis to further analyze and quantify the motion of the fish. The fish is seen as an oscillating structure, and the many degrees of freedom are the positions of points along the midline of the fish. The method applied is a complex orthogonal decomposition [8], which is a generalization of proper orthogonal decomposition [9]. The purpose is to demonstrate how the analysis method can be applied to fish motion data. In this example we look at a brief moment of swimming of an individual fish, rather than assess an average representation of swimming patterns of all whitings, and compare the movements of the fish with and without its tail fin.

The contributions of this work are in the description of animated fish swimming motion in terms of complex modes and modal coordinates and in providing an analysis tool for extracting this modal information from images. This new perspective enables a thorough and compact representation for fish kinematics.

**1.1 Background on Fish Kinematics.** Brief historical accounts [10,11] mention early studies, for example, by Aristotle, who thought the fish propelled themselves with their pectoral (side) fins, and by Borelli, a disciple of Galileo, who showed that the fish he studied could swim without the pectoral fins and instead relied on motions of the tail. Pertinent interest in fish motion has emerged since the start of the 20th century. Modern analyses began with Breder [12], who classified body/caudal-fin swimming motions. The classifications of undulatory swimming still used today range from anguilliform, subcarangiform, carangiform, thunniform, and/or ostraciform swimming [11,13,14]. The subjective descriptions of these motions vary progressively from large undulation in the anterior through posterior for anguilliform to subtle anterior motion in the subcarangiform motion to solely caudal (tail) fin motion in the thunniform motion. Lindsey [11] provided a chart comparing motion characteristics and body types associated with these classes of motion. Not all authors have used the same classifications.

In the 1930 s, Gray studied swimming fish in a set of important papers on fish locomotion [1,2,15]. In his work [1,2], he used a series of photographs, and interpretive sketches, to portray the movements of the bodies of various fish while swimming. In Ref. [2], he focused on the role of the caudal fin in the whiting species. The whiting is illustrated in Fig. 1. Gray experimented with the caudal fin's role by amputating the caudal fin of one whiting fish and comparing the swimming motion with its prior nonamputated (intact) motion. Gray had estimated that the caudal fin accounts for 40% of the intact fish's propulsion. However, he observed that the amputated fish did not swim at a significantly different speed than the intact fish and suggested that the amputated fish makes up for the lost caudal fin by changing its movement pattern so that energy is transferred by movement in the rest of its body.

Videler and Hess [14,16] sensed the motions of mackerel and saithe cinematographically, and processed the images into time series data, which were then analyzed in a variety of ways. They fit the motion at various locations, head to tail, on the body to Fourier series, including both sine and cosine terms. We'll come back to this later. Gillis [17] studied moving images of aquatic undulatory locomotion in fish and amphibians, in the spirit of Gray's work, and placed heavy emphasis on the effects of the tail angles while swimming.

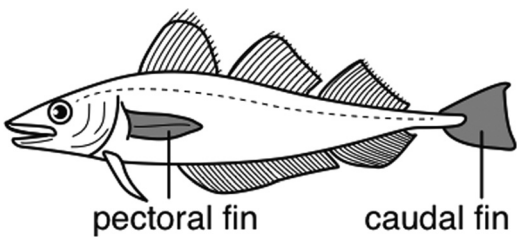


**Fig. 1 An illustration of the whiting**

[1]Corresponding author.

Contributed by the Design Engineering Division of ASME for publication in the JOURNAL OF VIBRATION AND ACOUSTICS Manuscript received October 24, 2011; final manuscript received September 8, 2012; published online February 25, 2013. Assoc. Editor: Thomas J. Royston.

  

Studying the body motions during undulatory swimming is important because the body kinematics are often used as input to computational models of the fluid flow around the fish. Wolfgang et al. [18] used experimental flow-visualization techniques to study the flow around a swimming giant danio and compared the experiments to a three-dimensional numerical model of the flow velocity field based on prescribed motions of the midline. Borazjani and Sotiropoulos, in a series of papers, modeled a virtual carangiform mackerel [19] and an anguilliform lamprey [20], each case numerically tethered at constant flow velocity, based on an incompressible Newtonian fluid modeled with the Navier–Stokes equations and solved by a hybrid Cartesian/immersed boundary method. Next they studied the effects of body shape and motion type [21]. In these studies, the imposed kinematics were quantified using a midline displacement function $h(x,t) = a(x)\sin(kx - \omega t)$, which describes a traveling wave with wave speed $c = \omega/k$ and spatially dependent wave amplitude $a(x)$, where $x$ is the position along the length of the fish, head to tail, $k$ is the wave number ($2\pi$ over wavelength), and $\omega$ is the oscillation frequency. In the anguilliform case, $a(x)$ was fit to an exponential function matching the data from Tytell and Lauder [22] based on American eels, and the wave number $k$ was set based on the value used for a robotic lamprey [4]. In the carangiform case, the wave amplitude $a(x)$ was expressed as a quadratic fit to the amplitude observations of Videler and Hess [16], with a wavelength based on studies by Videler and Wardle [23].

**1.2 Complex Modal Decomposition.** The method we use to analyze the motion of the fish is the complex orthogonal decomposition (COD), developed for structures [8] and since applied to the movements of worms [24] and waves in beams [25]. COD is a generalization of the well-known proper orthogonal decomposition (POD). POD, similar to singular value decomposition (SVD) and principal components analysis (PCA), is a tool for extracting modes that optimize the signal energy distribution in a set of measured time series. It has been used to characterize spatial coherence in turbulence and structures [9,26,27], the dimension of the dynamics [26,28,29], empirical modes for reduced order models [30,31], and in system identification [32,33]. POD, SVD, and PCA have been compared for structural applications [34]. In specific circumstances, the POD produces the normal modes of a structure [35–38]. POD is particularly useful if extracting standing wave components but is less suited for decomposing nonstanding wave components. The COD leads to complex modes that can be used to describe nonstanding and traveling waves.

SVD has been used to study the fluid wake of a fish [39]. In contrast, our work focuses on the body. Both COD and SVD are able to dissect the motion into modes and indicate a measure of energy associated with the modes.

The application of COD involves solving the eigenvalue problem $\mathbf{Rw} = \lambda\mathbf{w}$, where $\mathbf{R}$ is a complex "correlation matrix" built from time history measurements of a structure, in this application, the transverse displacement measurements along the body of the fish. The eigenvectors $\mathbf{w}$ of $\mathbf{R}$ are called "complex orthogonal modes" (COMs), and indicate mode shapes that represent the characteristic movement of the fish. The eigenvalues $\lambda$, which are the "complex orthogonal values" (COVs), indicate the mean squared amplitude of modal coordinates. The largest COV corresponds to the dominant waveform of the swimming fish. Using the results of COD, we will then be able to calculate other important information of the swimming mechanics of the fish, such as frequency and wave number (or wavelength). Other geometric properties of the mode could also be quantified, such as the amplitude profile, and the tail angle of the fish as it swims through time, a quantity that Gillis [17] focused on.

In this paper, following Gray [2], we analyze the movement of an intact and an amputated fish. Image processing is first applied to images from Gray's 1933 paper [2]. Transverse deflections of the midline of the fish are determined and become the subject of this analysis. Indeed, Gray's results of more than 75 years ago still contain information that becomes accessible as new analysis techniques are developed.

## 2 Methods

Gray's papers [1,2] incorporated photos of multiple species of fish as they swam through time. For this study, we focused on the photos of the movement of the whiting, before and after amputation [2]. The analysis in this work involved image processing to convert Gray's photographs of swimming fish into displacement data of the midline of the fish. The COD was then applied to the transverse displacement data. In this section, we discuss our process for obtaining transverse deflection data and then the decomposition analysis.

**2.1 Image Processing.** The whiting images were taken every 0.05 s [1] and were placed over 7.62 cm (3 in.) square grids so that the various positions of the fish could be easily compared. Inspection of the photos shows that the intact fish was about 30.48 cm (12 in.) in length, while the amputated fish was about 26.7 cm (10.5 in.) long.

The photos of the fish were scanned from Gray's paper [2] at a resolution of 118 pixels per cm (300 pixels per in.). Individual fish images were created with a common background, based on the grid in the original images, to provide a fixed coordinate system. Approximate midlines of the bodies of all individual fish images were created manually with Adobe Illustrator (Fig. 2). This

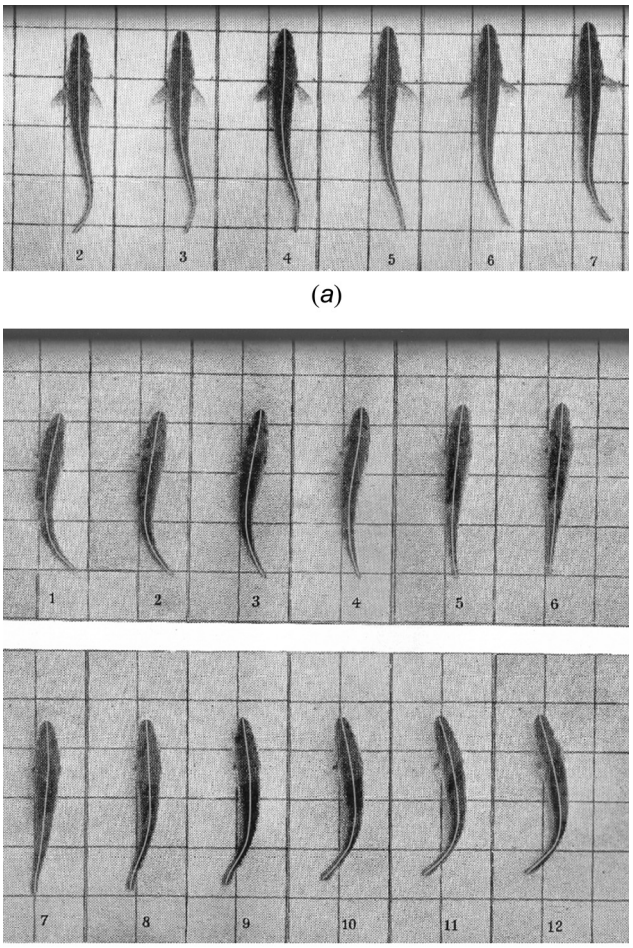


**Fig. 2 A sample of midlines superposed onto fish images obtained from Gray [2]. (*a*) Prior to tail amputation. (*b*) After amputation.**

manual approach seemed to produce cleaner transverse displacement data than did our attempt to use programmed image processing methods. It is expected that small errors incurred at this step will be modally filtered by the COD [24]. The midlines were then saved as black-and-white images. Representing each fish image, each computer-generated midline was loaded into a MATLAB program. This program assigned each pixel of the midlines a value corresponding to black or white in an array. Each column and row of the image array represented an $\hat{x}$ coordinate and a $\hat{y}$ coordinate. The program recognized the $\hat{x}$ and $\hat{y}$ coordinates of the midline pixels. The length of the midline was determined, and then the $\hat{x}$ and $\hat{y}$ coordinates of $m$ equally spaced virtual markers were established along the midline. The idea of using virtual markers on images of an organism follows work on the motion studies of nematodes [40,41]. The intact whiting was tagged with $m = 49$ virtual markers, while the amputated whiting had $m = 43$ virtual markers, such that the virtual markers were spaced by approximately 6.35 mm (0.25 in.) from head to tail.

A set of virtual marker locations was assembled for each fish image, thereby producing $\hat{x}$ and $\hat{y}$ time histories for each virtual marker. In the computations, the fish images were essentially oriented with a horizontal fish axis (a 90-deg counterclockwise rotation of the images shown in the figures), and so the $\hat{x}$ coordinate information is referred to as "axial," and $\hat{y}$ coordinate information is referred to as "transverse." The positions of the virtual markers were then used to monitor the fish's movements as it swam.

Gray's set of photographs of the intact whiting represented slightly more than a full cycle. Close inspection of these images suggested that the fish spent about the first half cycle swimming nearly straight forward. During the second half cycle, the right pectoral fin flipped forward and pulled back while the heading veered slightly to the left. Our aim is to quantify its straight forward locomotion pattern through one cycle. Henceforth, we incorporated the first half cycle, assumed symmetry, and regenerated the second half cycle, thereby obtaining a single cycle of dominantly straight forward locomotion. From further inspection and trial decompositions, we determined that six images (we used the first six snapshots) best approximated a half cycle, such that $n = 12$ for a full cycle.

Gray's photographs of the amputated whiting depicted slightly more than a *half* cycle of motion. Assuming symmetry between two half cycles of motion, we reconstructed the second half cycle to create a full cycle of motion. We used the data from images 2 through 11, such that the half cycle included 10 data, and thereby $n = 20$ for a full cycle of amputated fish motion.

We completed both motion cycles by taking the images of the first half cycle of motion and duplicating them by flipping them about the neutral axis of swimming. As such, the second half cycle was a mirror image of the first half cycle. If the transverse deflection data were flipped about an arbitrary axis, the oscillatory motion of the virtual markers would undergo jumps at the half cycle instants. To prevent this distortion, the neutral axis of swimming was determined by finding the mean of the marker positions at the first and seventh time samples (for the intact swimmer). If the sampling is nearly commensurate with the oscillation period, the seventh sample would represent the start of the second half cycle, and would serve as the cyclic opposite of the first sample, regardless of the phase of the oscillation. Thus, a marker's neutral position was approximated as the mean of the first and seventh time samples (for the intact fish). The neutral axis values of each virtual marker was subtracted from its half-cycle time series, so that the transverse data neutral axis was translated approximately to $y = 0$, and then the data were reflected about the new neutral $x$ axis to complete the cycle. (Another option for determining the neutral axis would be to fit a line to the means of the half cycle endpoints. In this case, the virtual marker neutral axis points had a very small variation with a trend, instead of a random distribution, and so the marker means themselves were used.) The neutral axis was a constant axis, and therefore, the resulting full cycle of transverse motion remained in a fixed Newtonian $(x, y)$ frame.

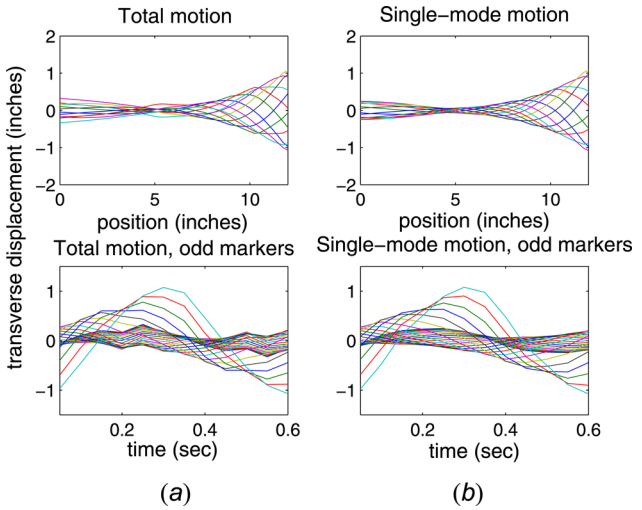


**Fig. 3 Intact fish transverse displacements. The top shows snapshots of all the midlines of the intact whiting through one full cycle (from two half cycles). The bottom shows time traces of the odd virtual markers. Column (*a*), after image processing, and (*b*) using only the dominant mode acquired after COD.**

A superposition of one cycle of samples of the fish markers, after the treatments above, is shown in the upper half of Fig. 3(*a*) for the intact fish, and Fig. 4(*a*) for the amputated fish. The lower half of Fig. 3 shows the transverse displacements of the odd virtual markers of the intact fish as functions of time. The large oscillations of tail motion and the smaller amplitude oscillations of markers on the body are apparent, as are the relative phases of oscillation, which show increasing lag toward the tail.

Drawings by Gray [2] rendered from his photographs show body movements relative to the anterior of the fish body. To draw comparisons between our results and Gray's observations, we also prepared transverse deflections relative to the fish's anterior. The fish is clearly not rigid, so this body-fixed deflection was estimated. Noting that the flexure of the anterior of the body was small, we fit a straight line to the first 20 markers in both the intact and amputated motions. The flexural deflections transverse to the "anterior-body-fixed" axis were then estimated with an assumption that the body angle was small.

**2.2 Complex Modal Decomposition.** A one-dimensional COD was applied solely to the transverse data of the fish. To apply COD, we first needed to convert the sampled real transverse oscillations $\mathbf{y}(t)$ into complex analytic signals $\mathbf{z}(t)$. We did this by the half-spectrum inversion method, in which the Fourier transform $\tilde{Y}_k(\omega)$ of each signal is digitally approximated by the fast Fourier transform (FFT) and then multiplied by two. The values

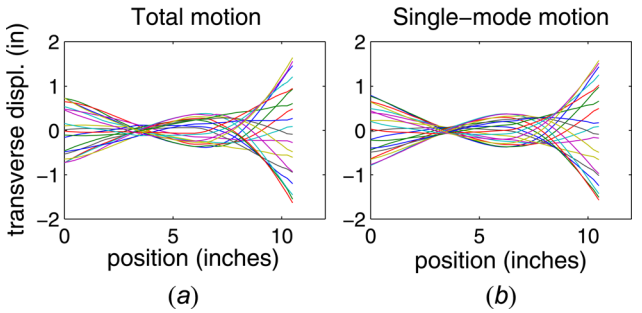


**Fig. 4 (*a*) Snapshots of all the midlines of the amputated whiting through one full cycle (from two half cycles) after image processing. (*b*) Representations of the midlines using only the dominant mode acquired after COD.**

of $2\tilde{Y}_k(\omega)$ at the negative frequencies are then set to zero to produce the one-sided $\tilde{Z}_k(\omega)$, and the inverse FFT is applied to obtain $z_k(t)$ [8,42]. The complex analytic signals $z_k(t)$ can also be obtained by applying the Hilbert transform to $y_k(t)$ to get $y_{Hk}(t)$, and then building $z_k(t) = y_k(t) + iy_{Hk}(t)$ [8,42].

The $\mathbf{z}(t)$ vector, whose elements $z_k(t)$ represent signals for each virtual marker, when sampled through time, comprises the $m \times n$ complex ensemble matrix $\mathbf{Z}$ for transverse motion. The $i$th row of $\mathbf{Z}$ represents the time history of the $i$th virtual marker, and the $j$th column is the $j$th time sample. The $m \times m$ complex "correlation" matrix was then constructed as $\mathbf{R} = \mathbf{Z}\bar{\mathbf{Z}}^T/n$, where the overbar indicates a complex conjugate. Matrix $\mathbf{R}$ is Hermitian, so the eigenvalues (COVs) $\lambda_i$ are real and the eigenvectors (COMs) $\mathbf{w}_i$ are orthogonal (unitary), that is, $\bar{\mathbf{w}}_i^T\mathbf{w}_i = 1$ for two of the same normalized eigenvectors, and $\bar{\mathbf{w}}_i^T\mathbf{w}_i = 0$ for two different eigenvectors [8]. The rank of $\mathbf{R}$ is bounded by the minimum of $n$ and $m$, which in our case is $n$. As such, at most, $n$ meaningful modes can be expected. Indeed, fewer than $n$ meaningful modes are expected, as many modes tend to have insignificant participation and are noise dominated. Since our fish undergoes a single cycle of motion, we expect a mode corresponding to the fundamental frequency of undulation, with higher modes corresponding to harmonics, most of which will be small noisy contributions.

Once the COMs, $\mathbf{w}_i$, are obtained, we can look at the motion associated with these modes. The premise is that the total motion is a sum of modal motions (e.g., see Ref. [43]), such that, in ensemble form, $\mathbf{Z} = \mathbf{WQ}$, where the $\mathbf{W}$ is the complex "modal matrix" whose columns are the dimensionless normalized modal vectors $\mathbf{w}_j$, and the rows of $\mathbf{Q}$ are samplings of the complex "modal coordinates." Then, this complex modal coordinate ensemble is

$$\mathbf{Q} = \mathbf{W}^{-1}\mathbf{Z} = \bar{\mathbf{W}}^T\mathbf{Z}$$

Ensemble matrices $\mathbf{Z}$ and $\mathbf{Q}$ both have units of length. Reduced modal motion can be constructed as $\mathbf{Z}_r = \mathbf{W}_r\mathbf{Q}_r$, where $\mathbf{W}_r = [\mathbf{w}_1, \ldots, \mathbf{w}_r] \leq$ is $m \times r$, $r < m$, and the rows of $\mathbf{Q}_r$ are samplings of the associated modal coordinates $q_j(t)$, $j = 1, \ldots, r$. Then $r \times n$ matrix $\mathbf{Q}_r = \bar{\mathbf{W}}_r^T\mathbf{Z}$, and hence,

$$\mathbf{Z}_r = \mathbf{W}_r\bar{\mathbf{W}}_r^T\mathbf{Z} \tag{1}$$

is the $m \times n$ modally reduced motion ensemble. If a small number of modes are "active," then $\mathbf{Z}_r \approx \mathbf{Z}$. This process can be used as a filter to "purify" the response based on the deterministic modal activity. The modal filter is not perfect because noise will also infiltrate the dominant modal coordinates. But the modal filter can be effective.

It may be useful to sketch an interpretation of a complex modal motion. The harmonic motion in a complex mode $\mathbf{z}_1(t) = e^{\alpha t}\mathbf{u}$, where $\mathbf{z}_1$ is a vector of complex analytic particle positions, $t$ is time, $\alpha = \gamma + \omega i$, and $\mathbf{u} = \mathbf{c} + \mathbf{d}i$ is a complex mode, with $\gamma, \omega, \mathbf{c}$ and $\mathbf{d}$ being real scalars and vectors, can be expressed in real form (for example, by combining with its complex conjugate, $\bar{\mathbf{z}}_1(t)$) as

$$\mathbf{y}_1(t) = e^{\gamma t}[\cos(\omega t)\mathbf{c} - \sin(\omega t)\mathbf{d}] \tag{2}$$

Thus, a complex mode induces an oscillation with a continual cyclic transition between the shapes $\mathbf{c}$ and $\mathbf{d}$. The relative sizes and degree of independence of $\mathbf{c}$ and $\mathbf{d}$ dictate the "amounts" of standing and traveling in the wave.

Indeed, the work of Videler and Hess [14,16] on the kinematics of saithe and mackerel was founded on a similar concept, without the terminology "complex modes." Videler and Hess expressed the motion in a Fourier series comprised of discretizations of associated functions $c_j(x)$ and $d_j(x)$, which play the role of real and imaginary part vectors $\mathbf{c}$ and $\mathbf{d}$, as coefficients of time varying harmonic terms $\cos(j\omega t)$ and $\sin(j\omega t)$ for a given point $x$ along the midline. In their work, the elements of vectors $\mathbf{c}$ and $\mathbf{d}$ were estimated from measurement Fourier coefficients and splines for up to three odd harmonics. The COD presented here is a method of efficiently packaging a similar estimation using complex modal vectors that result from an eigenvalue problem.

The nondimensional nonsynchronicity index, or "traveling index" for mixed traveling waves, quantifies the independence between the real and imaginary parts $\mathbf{c}$ and $\mathbf{d}$ of a COM as the reciprocal of their relative condition number. A traveling index value of zero indicates no independence between the real and imaginary vectors, thus, a standing wave and a traveling index value of 1 represents complete independence between the two vectors, meaning a "fully" traveling wave [8].

Furthermore, we can dissect the COM vector as $\mathbf{w} = \mathbf{w}_s + \mathbf{w}_t$, where $\mathbf{w}_s$ is a purely standing addend, and $\mathbf{w}_t$ is a purely traveling (or nonsynchronous) addend. Then $\mathbf{w}_s = \mathbf{c}_s + i\mathbf{d}_s$ and $\mathbf{w}_t = \mathbf{c}_t + i\mathbf{d}_t$. For example, if $\|\mathbf{c}\| \geq \|\mathbf{d}\|$, then the standing addend of $\mathbf{d}$ is the vector addend that is parallel to $\mathbf{c}$, such that $\mathbf{d}_s = \mathbf{d} \cdot \mathbf{e}_c\mathbf{e}_c$, where $\mathbf{e}_c = \mathbf{c}/\|\mathbf{c}\|$ is the unit vector in the direction of $\mathbf{c}$. Then the traveling vector addend of $\mathbf{d}$ is $\mathbf{d}_t = \mathbf{d} - \mathbf{d}_s$, which is the part that is normal to $\mathbf{c}$. The traveling addend of $\mathbf{c}$ is the piece of $\mathbf{c}$ of the same size as $\mathbf{d}_t$, such that $\mathbf{c}_t = \|\mathbf{d}_t\|\mathbf{e}_c$. Finally, the standing part of $\mathbf{c}_s = \mathbf{c} - \mathbf{c}_t$. Then the modal motion

$$\mathbf{Z}_r = \mathbf{wQ}_1 = \mathbf{w}_s\mathbf{Q}_1 + \mathbf{w}_t\mathbf{Q}_1 = \mathbf{Z}_s + \mathbf{Z}_t$$

is now separated into standing and traveling parts. (This breakdown is not unique, and there may be a way to optimize it.)

The eigenvalues $\lambda$ of $\mathbf{R}$ produce mean squared *amplitudes*, in units of length squared, of the modal coordinates. Examination of the $\lambda_j$ can indicate how many modes are active and significant. Since $\bar{\mathbf{w}}_j^T\mathbf{w}_j = 1$, the average of the mean amplitude squared of the markers on the fish is $\lambda_j/m$. Thus, $\lambda_j/m$ provides an estimate of the mean modal amplitude squared of deflection along the midline of the fish (see also Ref. [24]). The eigenvalues can also be used as indicators of the modal "signal energy."

COD can be performed with the goal of isolating a single mode of interest, and then representing the mode by the real and imaginary parts of the extracted complex mode, quantifying the motion parameters based on the complex mode and modal coordinate, enabling visualization and computation of additional quantities of interest, and "purifying" or isolating the motion in terms of the extracted mode. This is the aim of the current study. Another goal of COD can be to extract multiple modes and study properties of the modal spectrum, which can be a topic of future study for fish movement.

## 3 Results

We applied the image processing, data analysis, and COD, as discussed above, to both the intact and amputated fish in Newtonian and anterior-body-fixed frames. This section shows results of the COVs, COMs, and further analysis including the use of the modal coordinates.

**3.1 Newtonian Frame.** The COVs were used to establish modal dominance. For the intact whiting fish, the primary COV had a value of 51.5 $cm^2$ (7.98 $in^2$), and the next highest values were 0.716 $cm^2$ (0.111 $in^2$) and 0.0497 $cm^2$ (0.0077 $in^2$). The rest of the COVs were well below $10^{-13}$ $cm^2$. As such, the primary mode dominated with 98.5% of the signal energy. The scaled $\lambda_j/m$ indicates a mean squared amplitude of 1.05 $cm^2$ (0.163 $in^2$) on average per marker, or a root mean squared amplitude of about 1.03 cm (0.404 in.) on average per marker. The dominant swimming mode may contain effects of the fish's small deviation from steady swimming, and errors of the digitization of the photographic images. If it is part of a nonlinear mode, the second mode may include higher-order information about the mode. It may also contain effects of the fish's small deviation from steady swimming and errors of the digitization of the photographic images.

The COVs for the amputated whiting were 83.9, 0.826, 0.148, 0.0437, and 0.0217 $cm^2$, and smaller. Once again, the dominant

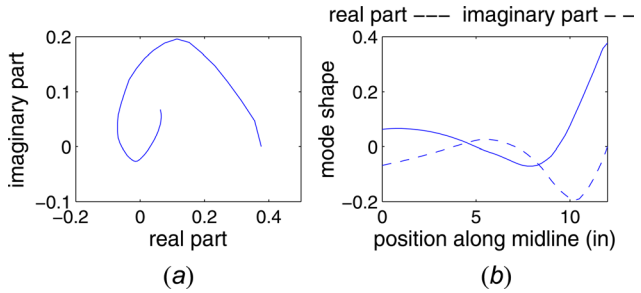


**Fig. 5 (*a*) Represents the dominant COM of the intact whiting in the complex plane. The endpoint close to the origin represents the head. (*b*) The real (solid line) and imaginary (dashed line) parts of the dominant COM, plotted against the fish midline.**

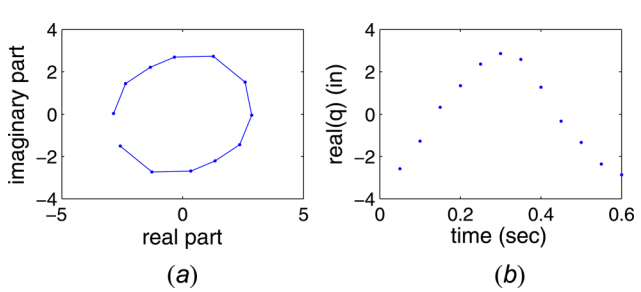


**Fig. 6 (*a*) The modal coordinate of the intact fish in the complex plane. (*b*) The real part of the modal coordinate versus time.**

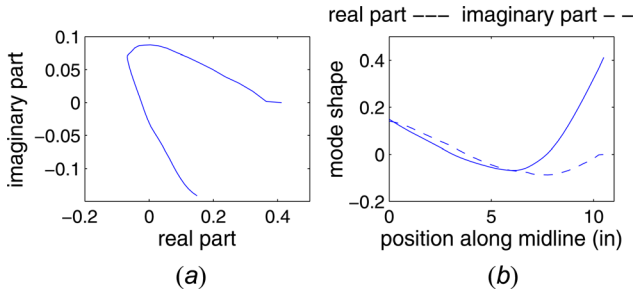


**Fig. 7 (*a*) The dominant COM of the amputated whiting in the complex plane. The lower endpoint represents the head. (*b*) The real and imaginary parts of the dominant COM plotted against the fish midline.**

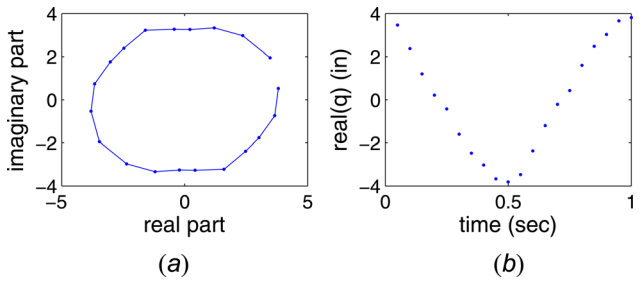


**Fig. 8 (*a*) The modal coordinate of the amputated fish in the complex plane. (*b*) The real part of the modal coordinate versus time.**

eigenvalues suggest that the amputated-fish motion can be well approximated by one mode, as the dominant mode had 98.8% of the signal energy. The dominant mode suggests a root mean squared amplitude of 1.40 cm (0.550 in.) on average per marker.

The eigenvector (COM) associated with the greatest eigenvalue (COV) corresponds to the shape of the dominant complex mode. For the intact fish, the dominant COM $\mathbf{w}_1$ in the complex plane, and also as both the real and imaginary parts of the complex mode, are plotted in Fig. 5. The traveling (or nonsynchronicity) index of the dominant mode for the intact whiting fish was 0.5205, which indicates significant, but not pure, traveling.

The first modal coordinate of the intact fish was extracted as $\mathbf{Q}_1 = \bar{\mathbf{w}}_1^T \mathbf{Z}$ and is plotted in Fig. 6 in the complex plane and as an oscillation via its real part. The complex modal coordinate goes through nearly a single period, as the next sample would come close to the starting point (and be part of the next cycle). This examination of the modal coordinate for various values of $n$ helped determine $n = 12$ as a nearly complete cycle of oscillation.

Applying the modal coordinate according to Eq. (1) produces the single-mode motion shown in Fig. 3(*b*). Comparison with Fig. 3(*a*) shows how noise from the raw motion is removed from the modally filtered motions. The modally filtered transverse displacement histories of the odd virtual markers results in a smoother motion in comparison with the raw marker-displacement histories of Fig. 3(*a*).

The dominant complex mode of the amputated whiting is shown in Fig. 7. Applying the modal coordinate according to Eq. (1) produced the single mode motion shown in Fig. 4(*b*). Again, comparison with the raw motions in Fig. 4(*a*) suggests that the motions are dominantly of a single mode and that small noise from the raw motions is removed from the modally filtered motions. The traveling index was 0.5209. The index suggests a similar amount of nonsynchronicity, which we take to be traveling, in the movements of both the intact and amputated fish in the Newtonian frame. We will discuss this later.

The first modal coordinate of the amputated fish is plotted in Fig. 8 in the complex plane and as an oscillation via its real part. Again, the complex modal coordinate goes through nearly a single period, as the next sample would come close to the starting point. This examination of the modal coordinate for various values of $n$ helped determine how many images to include in the complete half cycle. In comparison with the intact fish, the amputated fish modal coordinate shows a more sawtoothed waveform in the plot of the real part versus time (Fig. 8(*b*)).

We estimated the frequency, wave number, and wavelength, from the primary COM and modal coordinate. The frequency $f$ was estimated from the mean whirl rate of the dominant modal coordinate in the complex plane (Fig. 6(*a*)). The mean frequency through the full cycle for the intact whiting was $f = 1.6462$ cycles per second. This compares closely to the frequency of the nearly one-period time record of $1/(12\Delta t) = 1.6667$ Hz.

Wave speed $c$ can be estimated from estimates of frequency and wavelength $L$, as $c = Lf$. The wavelength can be obtained from an estimate of the wave number via $k = 2\pi/L$. Calculating the wave number was a delicate issue. The spatial waveforms are not harmonic and may not make a full cycle across the length of the fish. Particularly, that of the amputated fish seems to display only about a half cycle across the length of the fish. Inspection of the spacing of zero crossings of the real and imaginary parts of the intact whiting's complex mode suggests that the wavelength varies in space. Inspection of the real and imaginary parts of the amputated whiting's complex mode suggests that the two parts have different wavelengths. These features make it difficult to estimate the wavelength from the peak-to-peak characteristic of an oscillatory waveform, and points us toward estimating the local wave number from spatial local whirling rates as done in Refs. [24,25]. One whirl corresponds to a wavelength.

Estimating wavelength, if to be considered in relation to wave speed, may make more sense for the traveling part of the wave. Traveling and standing addends were separated and reanimated as $\mathbf{Z}_t = \mathbf{w}_t \mathbf{Q}_1$ and $\mathbf{Z}_s = \mathbf{w}_s \mathbf{Q}_1$ (in ensemble form) and are shown in Fig. 9 for the intact whiting. To the casual eye, the "traveling" addend in Fig. 9(*a*) does not seem to have a traveling advantage over the full modal oscillation shown in Fig. 3(*b*), but its traveling

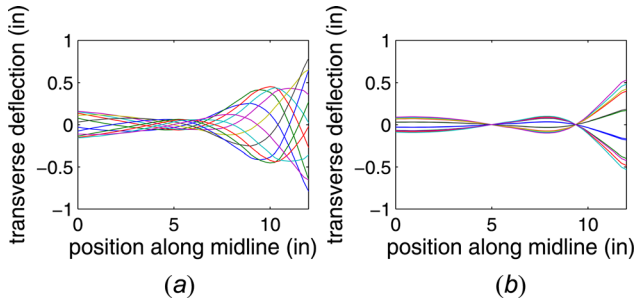


**Fig. 9 The separated traveling and standing parts of the fish motion. The superposed snapshots of (*a*) the traveling part of the primary modal motion of the intact whiting, and (*b*) the standing part of the primary modal motion.**

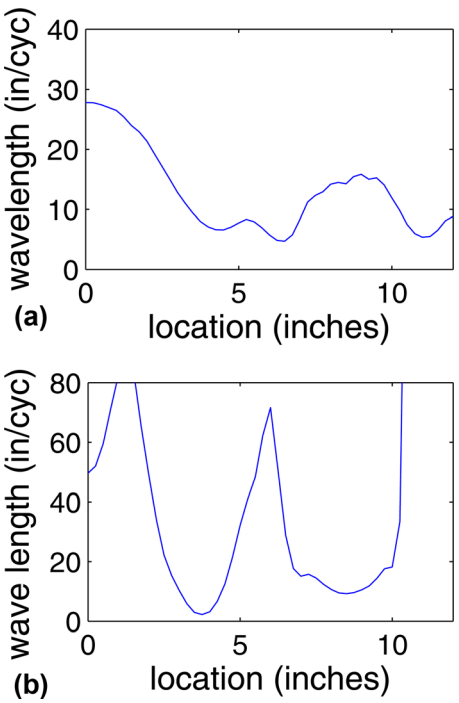


**Fig. 10 The local wavelength of the traveling part of the primary mode at each point along the midline of (*a*) the intact fish, (*b*) the amputated fish**

(nonsynchronicity) index of one is about double that of the full modal oscillation. The standing addend in Fig. 9(*b*) is clearly standing. The sum of these addends produces the motion in Fig. 3(*b*). The distribution of the local wavelength is shown in Fig. 10 for the traveling addend.

We sought wave number estimations of the normal swimming motions and found that the estimated wave number was not uniform. In the tail area, where we expect most of the thrust, the wavelength fluctuates around about 25 cm/cyc (10 in./cyc). The wave speed is then about 41 cm/s (16 in/s), well above mean observed speed of the fish (13 cm/s) for this interval of its swimming.

The mean frequency from the whirl rate of the amputated fish's complex modal coordinate was 0.9809 cyc/s, which is consistent with the frequency of 1.0 Hz that would be associated with a 20-image cycle. The separated traveling and standing aspects of the motion are shown in Fig. 11. Wavelengths obtained from the full complex mode and from the traveling addend (Fig. 10), calculated in the same way as for the intact fish, show large variability across the length of the fish. The mean full complex wavelength, which due to its coarseness may not be highly relevant for relating to the propulsion of the fish, was 76 cm/cycle, while that of the traveling

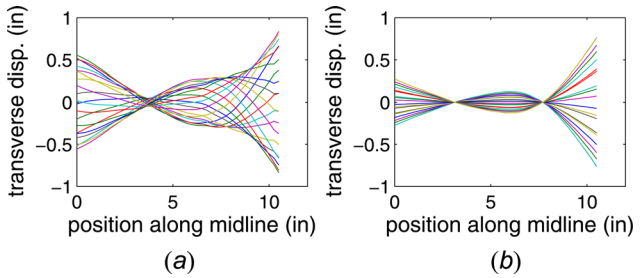


**Fig. 11 The separated traveling and standing parts of the amputated fish motion. (*a*) The reanimated traveling part of the primary modal motion, and (*b*) the reanimated standing part of the primary modal motion.**

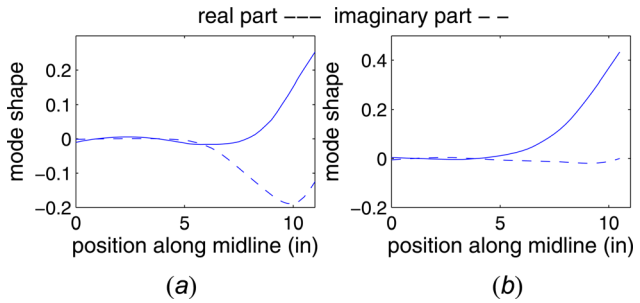


**Fig. 12 The real and imaginary parts of the primary mode of the deflections transverse to the anterior-body-fixed axis. (*a*) Intact fish, (*b*) amputated fish.**

addend was 89 cm/cycle, corresponding to mean wave speeds of about 76 and 89 cm/sec.

**3.2 Anterior-Body-Fixed Frame.** We also looked at decompositions from data in the anterior-body-fixed reference frame. The real and imaginary parts of the primary mode shapes of the intact and amputated fish are shown in Fig. 12. The traveling index of the intact fish's primary mode in the body fixed frame was 0.483, while that of the amputated fish was 0.0463, suggesting that, relative to the anterior of the body, the intact fish produces much more traveling in the waveform through its body than does the amputated fish. The highly standing nature of the primary mode of the amputated fish is also apparent in the figure, wherein the imaginary part is nearly zero. Modulation of the mode, then, is dominated by modulation of the real part.

The single-mode motions are shown in Fig. 13 as a superposition of the deflections transverse to the body-fixed axis in the upper graphs and time histories of these transverse deflections of the odd virtual markers in the lower graph. The propagation of a traveling wave is much more apparent in the intact fish than the amputated fish, both in the superposed transverse deflections and in the posterior marker histories.

## 4 Discussion

We saw that the estimated wavelength varies across the axis of the fish. Indeed, from Euler–Bernoulli beam theory, the wavelength is expected to be a function of frequency, dependent on beam parameters such as the Young's modulus $E$, area moment of inertia $I$, and mass density [44]. The fish is inhomogeneous, such that the values of $I$ and $E$ (should it be defined) would not be uniform. Thus, for a fish forced at a given frequency, it would not be unreasonable to produce an inhomogeneous wavelength. The roughly estimated wave speeds well exceeded the swimming speed.

Previous works on hydrodynamical modeling have used fish motion profiles with uniform wavelength and wave speed and an

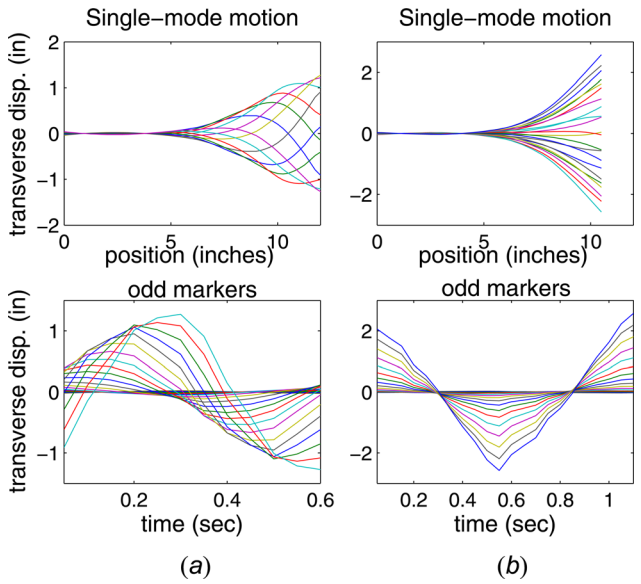


**Fig. 13 The single mode transverse deflections in a anterior-body-fixed frame. The top figures are superposed snapshots, and the bottom figures are odd marker histories, for columns (*a*) the intact fish, (*b*) the amputated fish.**

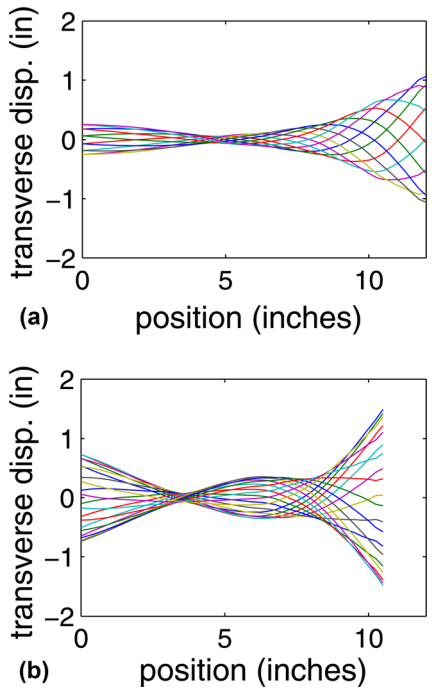


**Fig. 14 The single mode reanimated motion, based on a complex exponential modulation of the extracted dominant mode at the frequency defined by the mean whirl rate of the complex modal coordinate. (*a*) Intact fish, (*b*) amputated fish.**

experimentally observed amplitude $a(x)$ as a good first approximation, but the option of using complex modal oscillations may help in refinement of the hydrodynamical modeling. For this purpose, the motion can be reanimated using a complex exponential with the estimated frequency, modulating the complex mode shape, according to $\mathbf{y}(t) = \mathrm{Re}(Ae^{i2\pi\omega t})$, where $A$ is the square root of the COV, and $\omega$ is the identified modal frequency. A simulated transverse deflection is shown in Fig. 14 for both the intact and amputated fish. In this way, modal motions can be simulated indefinitely, at a time step of choice. Small motion axial effects can be easily incorporated by integrated foreshortening [24] of a nearly inextensible fish or by doing two-dimensional decompositions.

Gray made interesting observations from photos of the amputated swimmer. The absence of the caudal fin, according to Gray, did not inhibit the fish from swimming effectively, even though the motion was observed to be quite different. The intact fish swam at about 13 cm/s (5.2 in/s, or about one half length per second), while the amputated fish swam at about 11.7 cm/s (4.6 in/s). Gray made the subjective comment that he saw "very little evidence of a transmitted wave along the muscular tail." Gray's sketch of the animated motion of the amputated fish supports this comment, as the sketch shows the oscillation of the tail, relative to the anterior half of the body drawn fixed, visually indicates a standing wave. Our computations of the primary mode shape, and its traveling index, in the anterior-body-fixed frame also quantify and support Gray's comments, as do the visual single-mode features of Fig. 13. While the amputated fish did not produce the transmitted wave along the muscular tail, it produced a transmitted wavy motion relative to a fixed frame, in which the traveling index is significant, and the motion has significant traveling and standing addends. Indeed, Gray believed that the amputated animal generated thrust from the interaction of its body with the water as a result of its movement relative to a fixed frame. The whiting fish has a full set of dorsal and ventral fins (Fig. 1), and any action of these fins during the swimming motion has not been isolated from Gray's images nor referenced in Gray's paper.

Gray concluded that mechanical action of the water and caudal fin helps realize the traveling wave in the intact fish. We might speculate that while the caudal fin in the intact fish contributes thrust in the swimming direction of the nonamputated fish, it may act as a nonproportional damping element for the transverse deflection of the fish and thereby mechanically contribute to the complex nature of the mode. It may be worth considering that a strong swimming fish such as a carangiform swimmer may resonate the mode shape of its body in interaction with the water when swimming. Exploiting resonance may allow the fish to achieve significant oscillation amplitudes with minimal effort and thereby play a role in how the fish can swim efficiently.

Decompositions can be made under other variations in data was processing. When the transverse component of the fish centroid was removed from each frame, the modal motion (not shown) resembled that of Borazjani and Sotiropoulos [19] more closely.

Much of the interpretation of our results is dependent on the accuracy of the transverse deflections we obtained from the images and the conditions of Gray's work. For example, the single cycle of data from Gray [2], as it was noted by Videler [14], were obtained when the pectoral fins were extended, indicating that the fish was not swimming in its most efficient manner. Although limited data were used, the usefulness and feasibility of the approach can be seen. For this cycle of a given swimmer, a single mode was sufficient to represent the dominant characteristics of the transverse deflection of the midline. But we were not able to quantify long-term average swimming behavior of the fish. E. g., we do not capture modal characteristics during transient swimming, such as burst swimming or start up, turning, and breaking. Even with steady swimming, it would still be beneficial to examine large datasets. The computational tool is easily feasible for much larger time records, such as those in Refs. [24,25].

## 5 Conclusion

This work demonstrated the application of a modern vibration analysis tool to the photographic images of a swimming fish by Gray, thereby expanding on his studies of fish movement. We processed Gray's images to obtain transverse deflections of the midline of the fish and then conducted a complex modal decomposition to quantify the motion pattern. The method, applied in both the Newtonian frame and an anterior-body-fixed frame, enabled quantitative comparison between the swimming pattern

of a fish with and without its caudal fin. Interpretations of these quantities were consistent with Gray's subjective interpretations.

The decomposition produced a complex modal vector whose real and imaginary vector parts contain information on the mixed standing and traveling wave characteristics. In each case, intact and amputated, the motion was dominated by a single mode. Measurement noise and minor fluctuations were "modally filtered" and the single-mode motion was examined. The frequency of oscillation was cross checked using the complex modal coordinate. The complex mode and frequency can be used to reanimate the motion indefinitely at any time step. Results suggest a wavelength that varies with the location along the axis of the fish, which is not surprising if the fish is considered with reference to a nonuniform slender beam.

Quantifying the mechanics of the swimming motion serves multiple purposes. It gives us a better understanding of the motion of a fish as it swims, which is of value for the understanding of efficient water borne motion, application to biomimetic robotic locomotion, and for the knowledge and appreciation of fish themselves. The kinematics are important as input to fluid mechanics analyses. Perhaps the methods here can be applied as input in future refinements of hydrodynamical models.

In this work, new information was extracted from old images collected by Gray in the 1930 s. Computations also quantified and supported several of Gray's insights. The work demonstrates a method that can be added to the toolbox for quantifying fish kinematic parameters. It would be interesting, and feasible, to apply the method to longer time series data of transverse midline deflections during steady or unsteady swimming. Quantification of average steady behavior can be applied to classification of the types of swimming motion and its variation among species or even individuals.

## Acknowledgment

This material is spun off of work supported by the National Science Foundation under Grant No. CMMI-0727838. Bill Feeny, illustrator of the Zoology Department at the University of Wisconsin, provided the illustration of a whiting.

## References

[1] Gray, J., 1933,"Studies in Animal Locomotion I. The Movement of Fish With Special Reference to the Eel," J. Exp. Biol., **10**, pp. 88–111.
[2] Gray, J., 1933, "Studies in Animal Locomotion III. The Propulsive Mechanism of the Whiting (*Gadus merlangus*),". J. Exp. Biol., **10**, pp. 391–402.
[3] Morgansen, K. A., Triplett, B. I., and Klein, D. J., 2007, "Geometric Methods for Modeling and Control of Free-Swimming Fin-Actuated Underwater Vehicles," IEEE T. Robot., **23**(6), pp. 1184–1199.
[4] Hultmark, M., Leftwich, M., and Smits, A. J., 2007, "Flowfield Measurements in the Wake of a Robotic Lamprey," Exp. Fluids, **43**, pp. 683–690.
[5] McMasters, R. L., Grey, C. P., Sollock, J. M., Mukherjee, R., Benard, A., and Diaz, A. R., 2008, "Comparing the Mathematical Models of Lighthill to the Performance of a Biomimetic Fish," Bioinspir. Biomim., **3**(1), p. 016002.
[6] Epps, B. P., Alvarado, P. V. Y., Youcef-Toumi, K., and Techet, A. H., 2009, "Swimming Performance of a Biomimetic Compliant Fish-Like Robot," Exp. Fluids, **47**(6), pp. 927–939.
[7] Strefling, P., Hellum, A., and Mukherjee, R., 2012, "Modeling, Simulation and Performance of a Synergistically Propelled Ichthyoid," IEEE/ASME Trans. Mechatron, **17**(1), pp. 36–45.
[8] Feeny, B. F., 2008, "A Complex Orthogonal Decomposition for Wave Motion Analysis," J. Sound Vib., **310**(1–2), pp. 77–90.
[9] Lumley, J. L., 1970, *Stochastic Tools in Turbulence*, Academic Press, New York.
[10] Alexander, M. M., 1983, "The History of Fish Mechanics," *Fish Biomechanics*, Webb, P. W., and Weihs, D. eds., Praeger, New York, pp. 1–35.
[11] Lindsey, C. C., 1978, "Form, Function, and Locomotory Habits in Fish," *Fish Physiology, Locomotion*, Vol. 7, Hoar, W. S., and Randall, D. J., eds., Academic Press, New York, pp. 1–100.
[12] Breder, C. M., 1926, "The Locomotion of Fishes," Zoologica, **4**(5), pp. 159–297.
[13] Webb, P. W., 1978, "Hydrodynamics: Nonscombroid Fish," *Fish Physiology, Locomotion*, Vol. 7, Hoar, W. S., and Randall, D. J. eds., Academic Press, New York, pp. 190–315.
[14] Videler, J. J., 1993, Fish Swimming, Vol. Fish and Fisheries Series 10, Chapman and Hall, London.
[15] Gray, J., 1933, "Studies in Animal Locomotion II. The Relationship Between Waves of Muscular Contraction and the Propulsive Mechanism of the Eel," J. Exp. Biol., **10**, pp. 386–390.
[16] Videler, J. J., and Hess, F., 1984, "Fast Continuous Swimming of Two Pelagic Predators, Saithe (*Pollachius Virens*) and Mackerel (*Scomber Scombrus*): A Kinematic Analysis," J. Exp. Biol., **109**, pp. 209–228.
[17] Gillis, G. B., 1996, "Undulatory Locomotion in Elongate Aquatic Vertebrates: Anguilliform Swimming Since Sir James Gray," Amer. Zool., **36**, pp. 656–665.
[18] Wolfgang, M. J., Anderson, J. M., Grosenbaugh, M. A., Yue, D. K. P., and Triantafyllou, M. S., 1999, "Near-Body Flow Dynamics in Swimming Fish," J. Exp. Biol., **202**(17), pp. 2303–2327.
[19] Borazjani, I., and Sotiropoulos, F., 2008, "Numerical Investigation of the Hydrodynamics of Carangiform Swimming in the Transitional and Inertial Flow Regimes," J. Exp. Biol., **211**, pp. 1541–1588.
[20] Borazjani, I., and Sotiropoulos, F., 2009, "Numerical Investigation of the Hydrodynamics of Anguilliform Swimming in the Transitional and Inertial Flow Regimes," J. Exp. Biol., **212**, pp. 576–592.
[21] Borazjani, I., and Sotiropoulos, F., 2010, "On the Role of Form and Kinematics on the Hydrodynamics of Self-Propelled Body/Caudal Fin Swimming," J. Exp. Biol., **213**(1), pp. 89–107.
[22] Tytell, E. D., and Lauder, G. V., 2004, "The Hydrodynamics of Eel Swimming: I. Wake Structure," J. Exp. Biol., **207**, pp. 1825–1841.
[23] Videler, J. J., and Wardle, C. S., 1991, "Fish Swimming Stride by Stride: Speed Limits and Endurance," Rev. Fish Biol. Fisher., **1**(1), pp. 23–40.
[24] Feeny, B. F., Sternberg, P. W., Cronin, C. J., and Coppola, C. A., 2012, "Complex Modal Decomposition Applied to Nematode Posturing," ASME Computat. Nonlinear Dynam. (accepted).
[25] Feeny, B. F., 2012, "Complex Modal Decomposition for Estimating Wave Properties in One-Dimensional Media," ASME J. Vib. Acoust. (accepted).
[26] Berkooz, G., Holmes, P., and Lumley, J. L., 1993, "The Proper Orthogonal Decomposition in the Analysis of Turbulent Flows," Ann. Rev. Fluid Mech., **25**, pp. 539–575.
[27] Cusumano, J. P., and Bai, B.-Y., 1993, "Period-Infinity Periodic Motions, Chaos and Spatial Coherence in a 10 Degree of Freedom Impact Oscillator," Chaos Soliton Fract., **3**(5), pp. 515–535.
[28] Cusumano, J. P., Sharkady, M. T., and Kimble, B. W., 1994, "Experimental Measurements of Dimensionality Spatial Coherence in the Dynamics of a Chaotic Flexible-Beam Impact Oscillator," Philos. T. R. Soc. S-A, (1683), pp. 421–438.
[29] Epureanu, B. I., Tang, L. S., and Paidoussis, M. P., 2004, "Exploiting Chaotic Dynamics for Detecting Parametric Variations in Aeroselastic Systems," AIAA J., **42**(4), pp. 728–735.
[30] FitzSimons, P. M., and Rui, C., 1993, "Determining Low Dimensional Models of Distributed Systems," *Advances in Robust and Nonlinear Control Systems*, ASME-DSC53, pp. 9–15.
[31] Kerschen, G., Golinval, J. C., Vakakis, A. F., and Bergman, L. A., 2005, "The Method of Proper Orthogonal Decomposition for Dynamical Characterization and Order Reduction of Mechanical Systems: An Overview," Nonlinear Dynam., **41**(1–3), pp. 147–169.
[32] Yasuda, K., and Kamiya, K., 1997, "Experimental Identification Technique of Nonlinear Beams in Time Domain," ASME Design Engineering Technical Conferences, on CD-ROM.
[33] Ma, X., Azeez, M. A. F., and Vakakis, A. F., 2000, "Nonlinear Normal Modes and Nonparametric System Identification of Nonlinear Oscillators," Mech. Syst. Signal Process., **14**(1), pp. 37–48.
[34] Liang, Y. C., Lee, H. P., Lim, S. P., Lin, W. Z., Lee, K. H., and Wu, C. G., 2002, "Proper Orthogonal Decomposition and Its Applications—Part I: Theory," J. Sound Vib., **252**(3), pp. 527–544.
[35] Feeny, B. F., and Kappagantu, R., 1998, "On the Physical Interpretation of Proper Orthogonal Modes in Vibrations," J. Sound Vib., **211**(4), pp. 607–616.
[36] Feeny, B. F., 2002, "On the Proper Orthogonal Modes and Normal Modes of Continuous Vibration Systems," ASME J. Vib. Acoust., **124**(1), pp. 157–160.
[37] Kerschen, G., and Golinval, J. C., 2002, "Physical Interpretation of the Proper Orthogonal Modes Using the Singular Value Decomposition," J. Sound Vib., **249**(5), pp. 849–865.
[38] Feeny, B. F., and Liang, Y., 2003, "Interpreting Proper Orthogonal Modes in Randomly Excited Vibration Systems," J. Sound Vib., **265**(5), pp. 953–966.
[39] Ting, S. C., and Yang, J. T., 2009, "Extracting Energetically Dominant Flow Features in a Complicated Fish Wake Using Singular-Value Decomposition," Phys. Fluids, **21**(4), p. 041901.
[40] Feng, Z., Cronin, C. J, Wittig, J. H., Jr., Sternberg, P. W., and Schafer, W. R., 2004, "An Imaging System for Standardized Quantitative Analysis of *C. elegans* Behavior," BMC Bioinformatics, **5**, p. 115.
[41] Cronin, C. J., Mendel, J. E., Mukhtar, S., Kim, Y. M., Stirbl, R. C., Bruck, J., and Sternberg, P. W., 2005, "An Automated System for Measuring Parameters of Nematode Sinusoidal Movement," BMC Genetics, **6**, p. 5.
[42] Oppenheim, A. V., and Schafer, R. W., 1989, *Discrete-Time Signal Processing*, Prentice Hall, Englewood Cliffs, NJ.
[43] Meirovitch, L., 1997, *Principles and Techniques in Vibrations*, Prentice Hall, Upper Saddle River, NJ.
[44] Graff, K. F., 1975, *Wave Motion in Elastic Solids*, Ohio State University Press, printed at the Universities Press, Belfast.